communications earth & environment

Article

A Nature Portfolio journal

https://doi.org/10.1038/s43247-025-02086-7

Genesis and timing of KREEP-free lunar Mg-suite magmatism indicated by the first norite meteorite Arguin 002

Check for updates

Zilong Wang[1,2,3], Wei Tian[1] ✉, Wei-RZ Wang[2], Tabb C. Prissel[4], Yankun Di[5], Yuqi Qian[6], Ping-Ping Liu[1], Wenzhe Fa[1] & Ao Su[1]

There is ongoing debate about whether lunar magnesian suite (Mg-suite) magmatism was a global, nearly synchronous event with a genetic link to potassium, rare-earth element and phosphorus components (KREEP). Arguin 002, the first whole-rock meteorite classified as a lunar norite, offers a unique opportunity to explore the genesis and timing of Mg-suite rocks. Here we investigated the petrology, mineralogy, geochemistry, and chronology of Arguin 002, revealing it to be an evolved, KREEP-free Mg-suite rock with chemical similarities to atypical Apollo-15 Fe-norites. It likely formed through plutonic magmatism originating from low-degree partial melting of a deep, KREEP-free mantle source and has a $^{207}Pb/^{206}Pb$ age of 4341.5 ± 9.3 Ma. The potential source of Arguin 002 is within the South Pole-Aitken basin, near the Chang'e-6 landing site. These findings indicate that Mg-suite magmatism was a global and nearly synchronous event, potentially driven by rapid global mantle overturn.

Based on the current theories of the Moon formation, solidification of the lunar magma ocean (LMO) produced in the aftermath of the Moon-forming giant impact resulted in a chemically stratified lunar mantle consisting of mafic silicate cumulates (primarily olivine and orthopyroxene) and ilmenite-bearing Fe,Ti-rich cumulates, a low-density anorthositic lunar crust, and a uniform residuum interlayer that is rich in K, rare earth elements (REE), and P, known as urKREEP between the lunar crust and mantle[1–4]. This primordial differentiation was possibly followed immediately by density-driven overturn and partial melting of the cumulate mantle leading to secondary magmatism on the Moon such as the lunar magnesian-suite (Mg-suite) rocks (e.g.,[5,6]). The Mg-suite rocks, including dunites, troctolites, norites, and gabbronorites, represent a rare subset of lunar highland samples with endogenous igneous origin and compositionally distinct from the anorthositic rocks[1,4,7,8]. Most Mg-suite rocks appear as plutons intruded into the primary anorthositic lunar crust[8], while some of them may have erupted as lavas onto the Moon's surface[9].

The role of KREEP in the petrogenesis of Mg-suite rocks remains a long-standing enigma. Early studies highlighted that many Mg-suite rocks from the Apollo landing sites exhibit elevated trace element signatures, despite their high Mg# characteristic[10,11]. Consequently, a hybridized cumulate Mg-suite source containing a residual KREEP layer has been suggested[1,7,12,13]. However, the recent discovery of KREEP-depleted Mg-suite-related clasts in samples returned from other missions and meteorites has sparked debates on whether the petrogenesis of the Mg-suite rocks has to be KREEP-related[6,9,14–20]. Fractional crystallization of low-degree partial melts from KREEP-free mantle sources has been proposed as a mechanism to replicate the mineralogy of KREEP-depleted Apollo-15 Fe-norites, suggesting a potential new magmatic evolution trend on the Moon independent of KREEP[21]. Nonetheless, further research regarding detailed major- and trace-element analysis and modeling is essential to demonstrate the geological setting of this KREEP-free trend and its genetic connection to Mg-suite-related clasts in meteorites[5,22].

The spatial distribution and formation timing of Mg-suite rocks on the lunar surface also remain uncertain. Most Mg-suite samples collected by the sample-return missions are breccias, complicating efforts to determine their precise provenance. These rocks are hypothesized to be linked to nearside-specific magmatism associated with the Procellarum KREEP Terrane (PKT)[4]. However, remote sensing observations and geodynamic modeling suggest that Mg-suite rocks may be distributed globally across the Moon[6,8,23,24]. Furthermore, the radiometric ages of Mg-suite-related rocks collected at Apollo sites cluster around 4.33–4.36 Ga, hinting at a nearly contemporaneous formation[25,26]. If Mg-suite rocks are indeed globally

[1]School of Earth and Space Sciences, Peking University, Haidian, Beijing, China. [2]Institute of Geomechanics, Chinese Academy of Geological Sciences, Haidian, Beijing, China. [3]Institute for Geology, Mineralogy and Geophysics, Ruhr University Bochum, Bochum, North Rhine-Westphalia, Germany. [4]Department of Earth, Atmospheric, and Planetary Sciences, Purdue University, West Lafayette, IN, USA. [5]Department of Earth and Planetary Sciences, University of California, Davis, CA, USA. [6]Department of Earth Sciences and Laboratory for Space Research, The University of Hong Kong, Hong Kong, China. ✉e-mail: davidtian@pku.edu.cn

distributed, the 4.33–4.36 Ga interval may represent a global-scale magmatic event, necessitating further geochemical and chronological evidence from Mg-suite lithologies in meteorites. However, the linkage of meteoritic Mg-suite clasts to their Apollo bulk-rock counterparts in terms of petrogenesis is complicated by the lack of age constraints for meteoritic samples[7]. Additionally, Mg-suite samples identified in meteorites are typically small (e.g., 1–10 mm) clasts, and whole-rock compositions derived from these clasts may not accurately reflect those of their parent rocks, making it difficult to constrain their exact origins.

Officially approved on 19th March 2023, Arguin 002 is the first whole-rock sample in the lunar meteorite collection that has been compellingly classified as a norite (see Meteorite Bulletin Database). Arguin 002 is enveloped by a prominent, fresh fusion crust (Fig. 1), suggesting a recent landing and minimal terrestrial alteration. This research presents the detailed petrology, mineralogy, geochemistry, and U-Pb chronology of Arguin 002. Our results reveal that this meteorite is a chemically pristine but heavily-shocked, KREEP-depleted Mg-suite rock with a plutonic origin, formed contemporaneously with Apollo Mg-suite rocks but in geologically distinct locations. These findings can advance our understanding of the petrogenesis and spatial distribution of Mg-suite rocks beyond the PKT and shed light on the processes that triggered lunar Mg-suite magmatism.

Results

Petrology and mineralogy

Arguin 002 is primarily composed of orthopyroxene (47.2%), plagioclase (36.0%), and impact melt glass (9.8%). Lesser amounts of clinopyroxene (4.6%) and silica (2.1%) are also present (Fig. 1). Trace phases in the meteorite include merrillite, apatite, chromite, troilite, FeNi metal, ilmenite, and zirconium-bearing phases (Fig. 1).

Orthopyroxene and plagioclase in Arguin 002 are coarse-grained, both with typical sizes ranging from 1–5 mm. Some orthopyroxene grains may reach over 10 mm, as inferred from the near-complete parallelism of exsolved lamellae in these grains across the imaged area (Fig. 1). Clinopyroxene occurs exclusively as exsolution patches or lamellae within orthopyroxene, typically measuring 5–10 μm in width (Fig. 1). Most plagioclase grains have been transformed into maskelynite, and some pyroxene grains exhibit mosaic extinction under cross-polarized light, indicative of a high degree of impact metamorphism (Supplementary Fig. 1). The compositions of these primary minerals are homogeneous, with a range of $Wo_{3.2-4.7}En_{62.0-65.3}Fs_{30.8-34.0}$ for orthopyroxene, $Wo_{39.5-42.0}En_{42.0-44.0}Fs_{14.0-17.4}$ for clinopyroxene, and $An_{92.3-93.1}Ab_{6.4-7.2}Or_{0.4-0.6}$ for plagioclase. When plotted on a Mg# versus An# diagram (Fig. 2a), the mineral compositions of Arguin 002 fall into a gap between the typical Apollo Mg-suite lithologies and FANs, but overlapping with the compositions reported for "atypical" Fe-noritic clasts found in Apollo-15 regolith breccia[17] and Mg-suite-related clasts found in brecciated meteorites (Fig. 2a). Together, these data illustrate a steeper Mg-suite differentiation trend than is classically portrayed in Fig. 2a.

Impact melt glass is ubiquitously dispersed along inter-crystal boundaries and intra-crystal fractures (Fig. 1), with a composition resembling a mixture of plagioclase and pyroxene. Large, continuous impact melt glass can reach widths up to 1 mm, occasionally featuring elliptical bubbles (Fig. 1). The CaO/Al_2O_3 and MgO/Al_2O_3 ratios of the glass (Supplementary Fig. 2) support its impact origin.

Trace and accessory minerals are typically smaller in grain size and are commonly found in interstitial areas or hosted within the primary minerals (Fig. 1). Silica appears as anhedral crystals with a typical size of 200–500 μm, often associated with plagioclase and impact melt. Apatite and merrillite are often embedded in orthopyroxene or plagioclase, or associated with impact melt (Supplementary Fig. 3a, b). While typically sized between 5–20 μm, some merrillite grains are larger, reaching up to 30 × 200 μm in plagioclase. EPMA data confirm apatite as fluorapatite ($F_{0.76-0.86}Cl_{0.08-0.14}OH_{0.06-0.10}$), and merrillite containing trace amounts of Cl (~ 100 ppm). The zirconium-bearing phases in the sample include zircon, baddeleyite and zirconolite. Zircon grains are 30–50 μm in size, euhedral to subhedral, and usually coexist with plagioclase and silica (Supplementary Fig. 3c). Baddeleyite and zirconolite grains are relatively small, typically less than 5 μm (Supplementary Fig. 3d). FeNi metal and troilite grains are typically 2–10 μm in size, with Ni/Co ratios (0.96–2.85 for FeNi metal and 0.31–2.08 for troilite) consistent with those of indigenous metal/sulfides in pristine lunar rocks (Supplementary Fig. 4).

The bulk Na_2O and K_2O contents of the sample are below the alkali content threshold typical of alkali-suite rocks (> 0.1 wt% K_2O and 0.3 wt% Na_2O,[3]), confirming its classification as a Mg-suite rock. The bulk Mg# of the sample (65.4–68.6) indicates that it is too Mg-rich to be in equilibrium with its constituent pyroxene (Mg# = 65.5–69.0). This discrepancy suggests that the bulk composition does not represent the parental magma, consistent with the cumulate nature of the sample. Utilizing the partition coefficient $K_{Fe-Mg}^{opx-liq} = 0.28$, the Mg# of the parental melt calculated from bulk pyroxene ranges from 34.7 to 38.4. This value indicates that the parental magma of Arguin 002 is more evolved than most Apollo norites (parental magma Mg# = 36–60;[10]) and noritic clasts in meteorites (parental magma Mg# = 43–55;[18,27]). In contrast, the evolution extent of its parental magma is comparable to some of the evolved Fe-noritic clasts reported in the Apollo-15 regolith breccia[17].

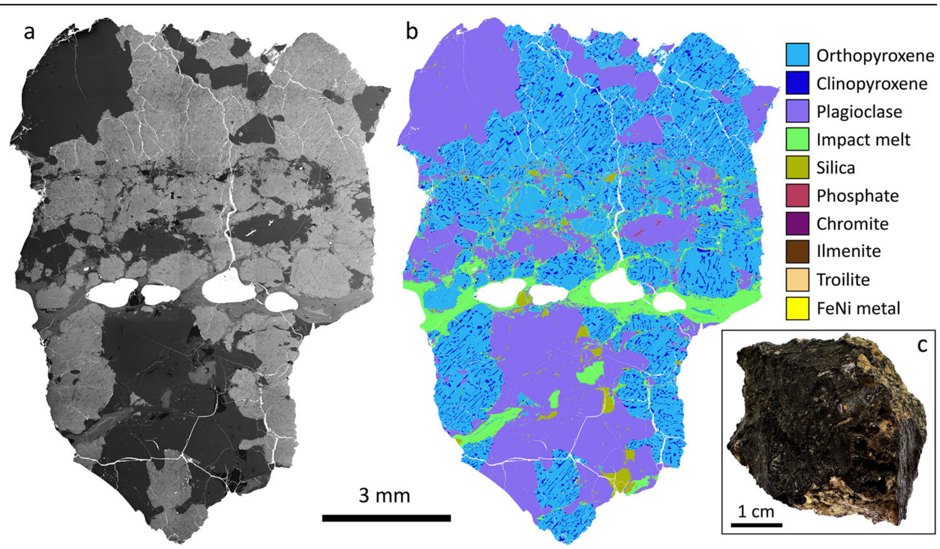

Fig. 1 | Macro and microstructure of the norite meteorite Arguin 002. **a** Mosaic backscattered electron (BSE) image of Arguin 002 with enhanced contrast, taken with TIMA. **b** Image depicting the mineral distribution in Arguin 002, taken with TESCAN Integrated Mineral Analyzer (TIMA). **c** Hand specimen photo of Arguin 002.

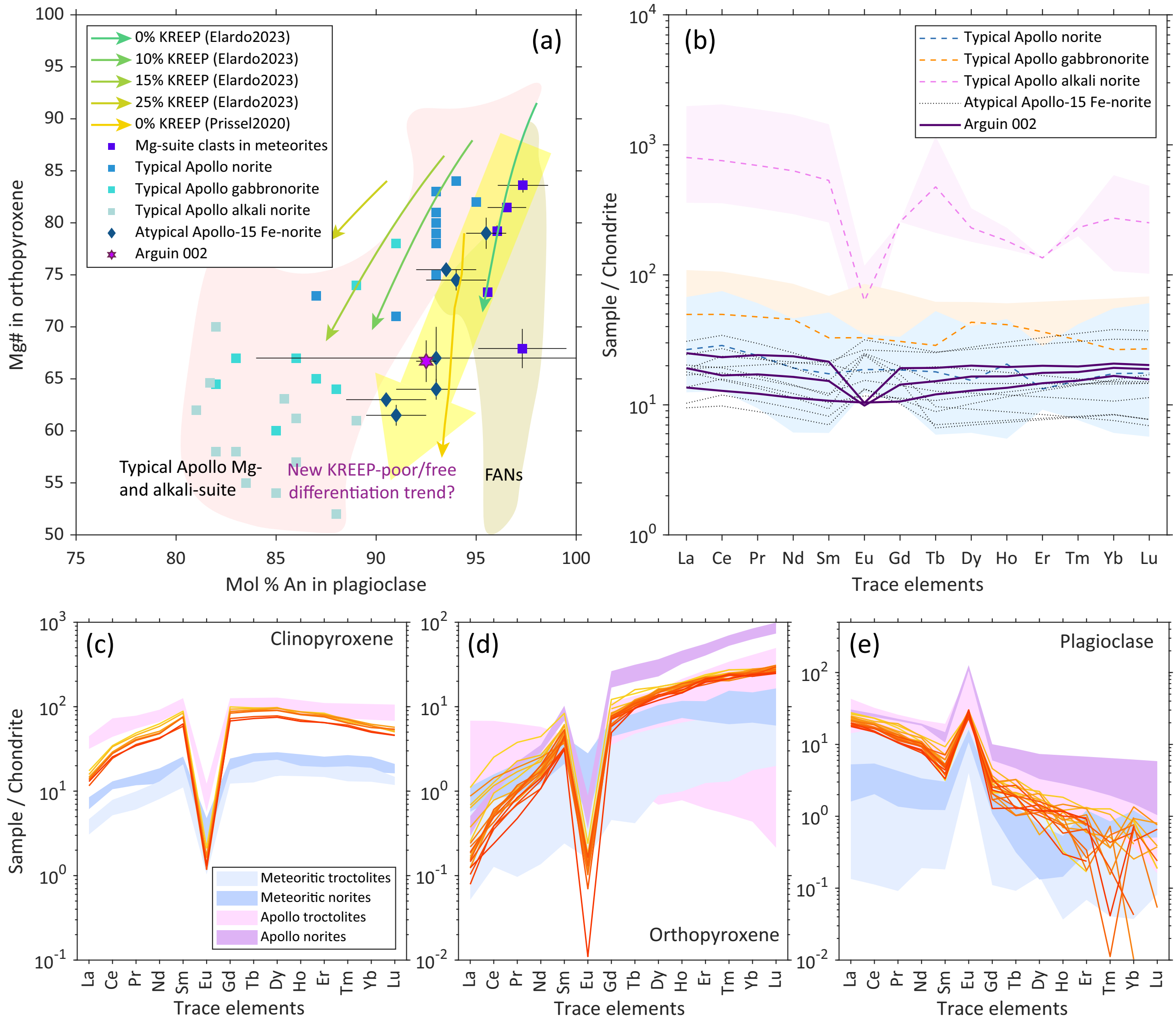

Fig. 2 | Major and trace element diagrams for the bulk rock and minerals of Arguin 002. a Mg# of orthopyroxene vs. An# in plagioclase for Arguin 002, Apollo norites/alkali norites/gabbronorites, atypical Apollo-15 Fe-norites, Mg-suite-related clasts in meteorites, and the compositional ranges of typical Apollo Mg- and alkali-suite, and ferroan anorthosites (FANs). Results from thermodynamic calculations for partial melts of Mg-suite analog sources with varying amounts of KREEP are represented by colored curves (Elardo2023:[31]; Prissel2020:[21]). **b** The bulk-rock rare-earth element (REE) pattern of Arguin 002, compared with those of typical Apollo norites/alkali norites/gabbronorites and atypical Apollo-15 Fe-norites. **c–e** The REE patterns of silicate minerals (clinopyroxene, orthopyroxene, plagioclase) in Arguin 002, compared with the compositional ranges of Apollo Mg-suite, FANs, and Mg-suite-related clasts in meteorites. The typical Apollo data in (**a**, **b**) and (**c**–**e**) are from[4] and[12] respectively. The Apollo-15 Fe-norite data are from[17]. Data of Mg-suite-related clasts in meteorites are from[15,18,20,27]. The compositional ranges (colored shades) in (**a**) are from Ref. 31.

Geochemistry

The bulk-rock trace-element contents of Arguin 002 measured in the three parallel analyses show moderate variation, with an enriched signature of La ~ 13.6–25.0 × CI to Lu ~ 15.7–20.2 × CI, accompanied by a flat to slight negative Eu anomaly. The chemical differences between the analyses are likely due to minor variation of phosphate abundances in the samples (Supplementary Fig. 5a). Despite this variation, the average rare-earth element (REE) content of Arguin 002 is similar to, but slightly depleted in light REEs compared to typical Apollo norites (Fig. 2b). Additionally, the REE content of Arguin 002 is on the same order of magnitude with some atypical Apollo-15 Fe-norites, which show enrichments of ~ 10–30 × CI (Fig. 2b).

Given the relatively low bulk concentrations of Sm (1.59–3.18 ppm) and Th (0.41–0.86 ppm), Arguin 002 is located near the conjunction line of feldspathic highland terrain (FHT) and maria on the bulk Sc-Sm and FeO-Th plots, distinguishing it from both known lunar meteorites and samples from return missions (Fig. 3). Furthermore, the bulk Ni/Co ratio (0.79–0.83) of the sample is among the lowest in lunar meteorites (Supplementary Fig. 6), indicating minimal meteoritic contamination and supporting the pristine nature of the sample.

The REE concentrations in the major minerals of Arguin 002 generally fall between those observed in the major minerals of Apollo Mg-suite samples and those in Mg-suite-related clasts found in lunar meteorites (Fig. 2c–e). Both clinopyroxene and orthopyroxene show pronounced negative Eu anomalies ($Eu/Eu^{*} = Eu_N/\sqrt{Sm_N \times Gd_N}$ = 0.01–0.02, subscript "N" refers to chondrite-normalized concentrations), suggesting substantial plagioclase fractionation of their parental magma (Fig. 2c, d). The impact melt glass has a slightly LREE-enriched pattern (La ~ 11–33 × CI, Lu ~ 9–18 × CI) and varying Eu anomalies (Eu/Eu^{*} = 0.5–3.0), consistent with mixtures of pyroxene and plagioclase in differing proportions (Supplementary Data 1). Apatite and merrillite are the primary REE hosts,

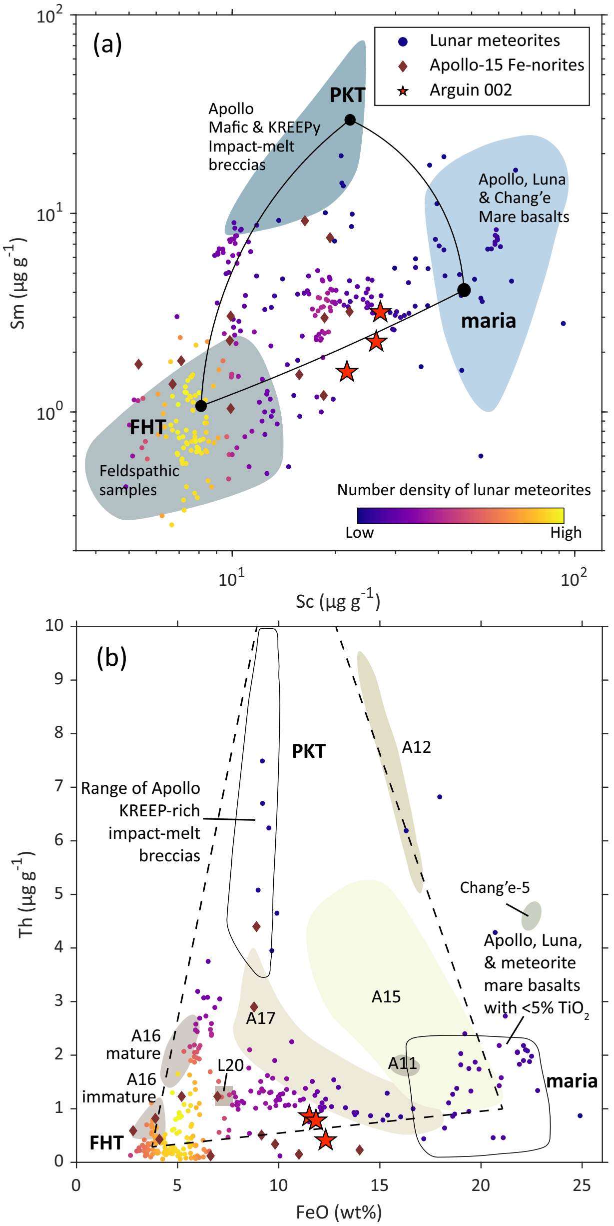

Fig. 3 | Representations of bulk compositional spaces for lunar samples. **a** Sm vs Sc diagram; **b** FeO vs Th diagram. The bulk composition of Arguin 002 is highlighted using orange pentagrams. Compositional spaces (FHT, PKT, maria) defined by returned lunar samples and the compositional data points of 278 lunar meteorites[71] and Apollo-15 Fe-norites[17] are plotted for comparison. A number-density plot technique is employed, where brighter colors indicate higher concentrations of data points, reflecting a greater number of meteorites in those regions. The diagrams are adapted from[71,72].

with La contents of 350–870 × CI for apatite and 46,000–47,000 × CI for merrillite, and Lu contents of 69–220 × CI for apatite and 4500–4800 × CI for merrillite. Both phases exhibit deep negative Eu anomalies (Eu/Eu^* = 0.02–0.08 for apatite; Eu/Eu^* = 0.003–0.006 for merrillite) (Supplementary Data 1). The uniformity of REE patterns and concentrations among grains of the same mineral phase suggests chemical equilibrium and inheritance from the parental melt, arguing against post-crystallization trace-element addition via metasomatism[10].

Chronology

U-Pb isotopic analyses were performed on four spots from two apatite grains, three spots from one zircon grain, and four spots from three merrillite grains. Those grains were chosen due to their sizes large enough for SIMS analyses with spot sizes of 4 μm. All the analyzed spots have U-Pb isotopic compositions (corrected for minor terrestrial common Pb based on ^{204}Pb) lying on or close to the Tera-Wasserburg concordia (Fig. 4a), confirming closed U-Pb systems with minimal Pb loss in the analyzed domains. The analyses yielded weighted mean ^{207}Pb/^{206}Pb dates of 4343 ± 17 Ma for apatite, 4335 ± 14 Ma for zircon, and 4280 ± 22 Ma for merrillite (Fig. 4b; uncertainties reported here and below are 95% confidence intervals calculated using Isoplot 3.75,[28]). The ^{207}Pb/^{206}Pb dates of apatite and zircon agree with each other within error, and together define a weighted mean date of 4341.5 ± 9.3 Ma, while the ^{207}Pb/^{206}Pb date of merrillite is resolvably younger than that of zircon and apatite by 62 ± 24 Ma.

Discussion

Evidence for a KREEP-free Mg-suite source region

Lunar Mg-suite rocks sampled during Apollo missions are typically enriched in trace elements, suggesting interactions with KREEPy reservoirs in their petrogenesis[8,12]. These rocks are retrieved from the lunar nearside and believed to have a genetic association with urKREEP. Potential mechanisms for the incorporation of the KREEP signature include melting of a hybridized lunar mantle or assimilation of urKREEP near the base of lunar crust during the magma ascent[5,8]. Prior studies[29,30] have also proposed that the cumulate lithologies of the Mg-suite may result from fractional crystallization of KREEP-like magmas. More recent thermodynamic modeling supports that typical Apollo Mg-suite rocks likely originated from sources with 10–25 wt% KREEP components[31].

In contrast, our analysis suggests that Arguin 002 was derived from a source region with considerably less KREEP content than typical Apollo Mg-suite rocks, based on the following observations: (1) The lower Mg# in both bulk rock and orthopyroxene of Arguin 002 indicates an evolved magma origin (Fig. 2a). Despite this evolved nature, the REE abundances in both the bulk rock (Fig. 2b) and mineral phases (Fig. 2c–e) are similar to or lower than those of typical Apollo norites, suggesting that its parental magma contained lower incompatible element concentrations (i.e., KREEP components). (2) The Sm and Th concentrations in Arguin 002 differ from those in typical Apollo samples (Fig. 3), pointing to a source region likely located far from the PKT, with minimal interaction with KREEPy materials[32,33].

Arguin 002, atypical Apollo-15 Fe-noritic clasts, and KREEP-free Mg-suite-related clasts from regolith meteorites define a steeper Mg-suite differentiation trend in orthopyroxene Mg# vs. plagioclase An# space, diverging from the canonical trend of typical Apollo Mg-suite rocks (Fig. 2a). Thermodynamic modeling of major-element evolution[21,31] suggests that this trend can arise from a primary magma formed without KREEP addition (Fig. 2a). Prissel & Gross[21] propose that KREEP-free Mg-suite lithologies form through high-degree (~ 50–87% for troctolites and > 87% for norites) fractional crystallization of a primary magma generated by low-degree (~ 1–2 wt%) batch melting of deep (2.1 GPa, equivalent to ~ 420 km in depth) primitive LMO cumulates. Given the similarities of Mg# and An# between Arguin 002 and Apollo-15 Fe-norites, the major-element compositional evolution of minerals in Arguin 002 could have formed through a similar process. Does the trace-element compositional evolution of minerals in Arguin 002 also support this scenario?

To explore the genetic relationships between KREEP-free Mg-suite lithologies and Arguin 002, we modeled trace-element partitioning during mantle melting and fractional crystallization. Results show that REE contents and patterns of KREEP-free Mg-suite-related clasts in lunar meteorites can be reproduced by ~ 80–95% fractional crystallization of olivine and plagioclase from a primary melt generated by 1% partial melting of a KREEP-free mantle source (Fig. 5). A little higher degree of fractionation (~ 95–97%) of this primary melt would yield an evolved magma with REE contents and patterns consistent with the parental magma of Arguin 002 (Fig. 5). By contrast, the REE abundances in Apollo Mg-suite parental magmas are too high to replicate through similar processes, indicating that their source regions likely contain notable amounts of KREEP (Fig. 5). These

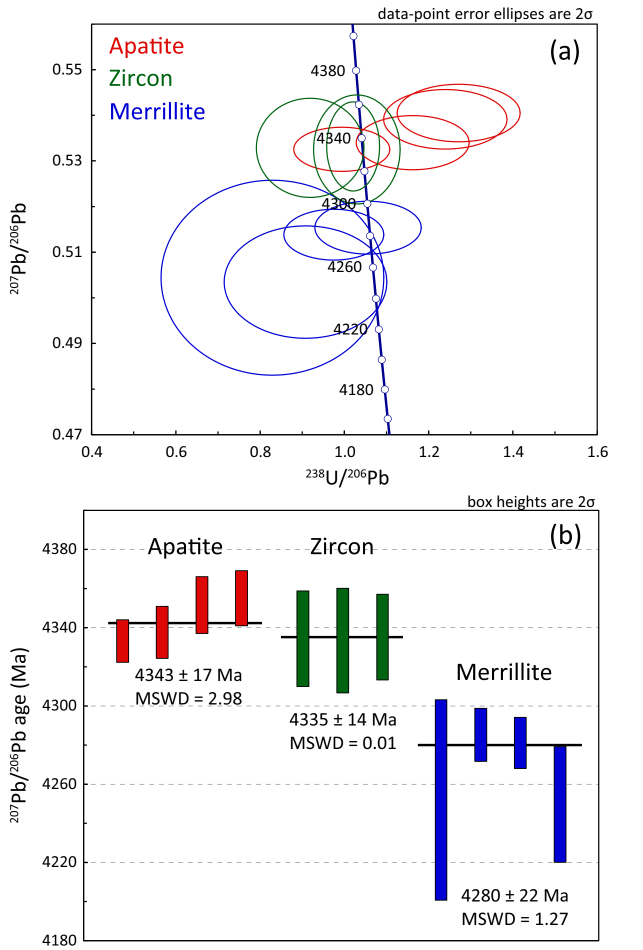

Fig. 4 | SIMS U-Pb dating results of Arguin 002. a Tera-Wasserburg plot of zircon and phosphate analyses. **b** Weighted mean $^{207}Pb/^{206}Pb$ ages for zircon and phosphates.

findings support the hypothesis that KREEP-free norites like Arguin 002 originated from a mantle region similar to that of KREEP-free Mg-suite-related clasts in meteorites but experienced higher degrees of fractional crystallization, resulting in the observed REE enrichment and deeper Eu anomalies.

In summary, our study suggests that Arguin 002 originated from a distinct KREEP-free Mg-suite source region, likely part of the primitive lunar lower mantle, composed primarily of KREEP-free olivine cumulates from LMO solidification[1,21]. KREEP-free Mg-suite magmatism would initiate through low-degree (< 2%) partial melting of this primitive source, followed by high-degree (> 90%) fractional crystallization of olivine, plagioclase, and orthopyroxene, forming KREEP-free lithologies such as troctolites and norites. The limited partial melting of the KREEP-free mantle source may explain the lower abundance of Mg-suite materials in the lunar highlands compared to the PKT region, which is consistent with recent remote-sensing findings[6]. Future radiogenic isotope analyses (e.g., Rb-Sr, Sm-Nd, U-Pb) will be crucial to confirm the KREEP-free nature of Arguin 002 and its source region.

The petrogenesis of KREEP-free Mg-suite rocks

The petrogenesis of lunar Mg-suite rocks remains a subject of debate. Current models for their origin can be grouped into three categories ([5] and references therein): (1) products of LMO crystallization, (2) solidification of impact melts, and (3) crystallization of partial melts derived from mantle regions at varying depths and KREEP contents, followed by emplacement into the deep crust or onto the lunar surface.

Model (1) is unlikely for Arguin 002, as its evolved whole-rock chemistry (Mg# = 65.4–68.8) and silica-bearing composition do not align with the Mg-rich (Mg# > 80) mantle lithologies hypothesized to result from LMO crystallization[2,7,34,35]. Additionally, Arguin 002 is unlikely to represent a major component of the lunar primordial lower crust, as Mg-rich noritic materials are not expected to directly derive from the LMO[36].

Furthermore, while some thermodynamic models support norite formation via fractional crystallization of impact melt from a mixture of mantle dunite (77–80 wt%) and crustal anorthosite (13–20 wt%)[37,38], this mechanism appears inapplicable to Arguin 002 for several reasons. First, the presence of coarse-grained pyroxene and plagioclase strongly indicates that Arguin 002 is a pristine plutonic rock rather than an impact melt product. Second, impact melts from such mixtures are typically plagioclase-saturated and favor Mg-Al spinel crystallization[39]. However, Arguin 002 contains chromite rather than Mg-Al spinel, indicating it could not have crystallized from these melts. Third, clinopyroxene thermobarometric calculations place the formation conditions of Arguin 002 at 0.6–1.0 kbar and 1129–1144 °C, corresponding to depths of ~12–20 km within the lunar crust (Supplementary Fig. 7). If Arguin 002 formed from a thick impact melt sheet at such depths, zirconium-bearing phases in the sample would exhibit microstructures indicative of reversion from a cubic-ZrO_2 phase, which forms at extremely high temperatures (> 2100 °C) characteristic of thick impact melt sheets[40]. However, no such microstructures were identified in Arguin 002 using Raman spectrometer. Fourth, the low Ni/Co ratios observed in both FeNi metal and the whole rock suggest minimal assimilation of impactor materials, further challenging the impact-related origin hypothesis.

The genesis of Arguin 002 is more consistent with endogenous magmatic processes occurring after the formation of the primordial lunar crust, similar to the model (3). The similarities in mineral compositions (Fig. 2a) and bulk-rock trace-element contents (Fig. 2b) between Arguin 002 and Apollo-15 Fe-norites possibly suggest a similar genesis through fractional crystallization of melts derived from magnesian LMO cumulates, with minimal KREEP involvement[21]. The bulk major- and trace-element differences (e.g., Eu anomaly, Sm, Sc, Th, and FeO contents) between Arguin 002 and Apollo-15 Fe-norites (Fig. 2b, 3) can be attributed to a higher modal abundance of plagioclase (50–80%) in Apollo-15 Fe-norites (Supplementary Fig. 5b), likely due to the earlier fractionation and accumulation of plagioclase relative to orthopyroxene, as well as potential sampling bias.

Given that Arguin 002 and related KREEP-free Mg-suite rocks most likely originated from deep-seated emplacement within the lunar crust, it is probable that this rock was transported to the lunar surface only during the formation of large impact basins, which possess the capability to excavate rocks from several kilometers within the crust (e.g.,[41]). Thus, we propose that the formation process of KREEP-free Mg-suite rocks involves the following stages: (1) low-degree (< 2%) partial melting of KREEP-free primitive magnesian cumulates in the lunar mantle to form the primary magma (Fig. 6a), possibly triggered by the mantle overturn; (2) diapiric ascent of the magma through the overlying anorthositic crust, forming Mg-suite cumulates at depths of ~12–20 km (Fig. 6b) following high-degree (> 80%) fractional crystallization of Mg-rich minerals and plagioclase; (3) transportation of the cumulates to the lunar surface by large basin-forming impact events (Fig. 6c); (4) subsequent smaller impacts ejecting the exposed troctolitic/noritic materials to Earth as meteorites (Fig. 6d). This implies that lunar Mg-suite magmatism is not necessarily driven by the radiogenic heating of KREEP components, but rather, can be caused by alternative endogenous processes.

The timescale and global distribution of Mg-suite magmatism

Radiometric dating of Arguin 002 provides essential constraints on the formation timeline of Mg-suite rocks. U-Pb dating of apatite and zircon in this study yields a consistent age of 4341.5 ± 9.3 Ma. We interpret this as the primary crystallization age of Arguin 002 for two reasons: (1) the well-defined Raman peaks and uniform contrast in cathodoluminescence images of apatite suggest minimal effects from post-crystallization shock processes

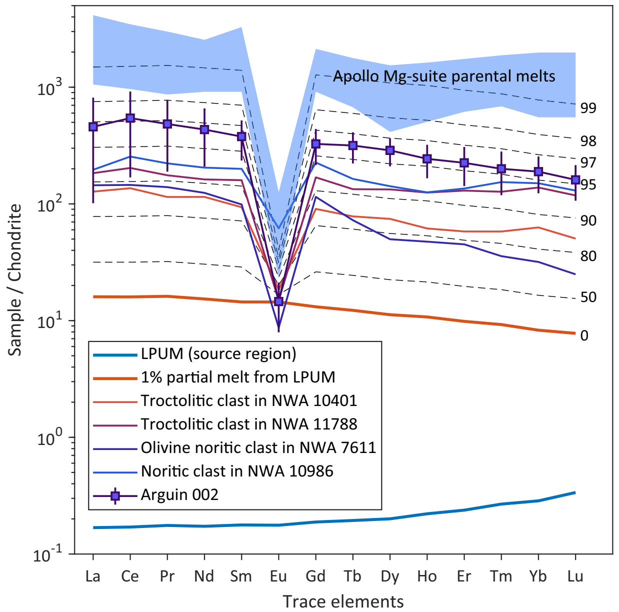

Fig. 5 | Trace-element partitioning behaviors of a KREEP-free lunar primary mantle source (LPUM) during partial melting and fractional crystallization. The figure displays modeled REE contents of the source region, 1% partial melts from the source, and evolved melts (dashed black curves) at varying degrees of fractionation. These are compared with calculated parental magmas of Mg-suite-related clasts from NWA 7611[27], NWA 10401[15], NWA 10986[18], and NWA 11788[20], illustrated with colored curves. The REE range for Apollo Mg-suite parental melts is sourced from[31]. Numbers adjacent to the dashed black curves indicate the fractionation degree for each evolved melt. Error bars represent 1σ uncertainties.

(Supplementary Fig. 8); (2) the analyzed zircon grain does not exhibit granular neoblastic recrystallization structure, indicating that it effectively preserved its original ^{207}Pb/^{206}Pb age during impact events (e.g.,[42,43]). Conversely, the younger ^{207}Pb/^{206}Pb age of merrillite (4279.6 ± 22.1 Ma) likely reflects impact-induced resetting. The presence of residual apatite within merrillite grains suggests that merrillite may have formed from the transformation of pre-existing apatite (Supplementary Fig. 3a, b) due to impact-induced shock compression[44].

High-precision isochron ages for Apollo Mg-suite rocks cluster between 4.33 and 4.36 Ga (e.g.,[7,25,45]), consistent with the ^{207}Pb/^{206}Pb age of Arguin 002 determined from zircon and apatite (Fig. 7). This synchronization suggests that Arguin 002 may have occurred concurrently with that of Apollo Mg-suite rocks. Through the comparison of bulk-rock data with lunar surface remote sensing spectral data, we have identified four potential source sites for Mg-suite rocks similar in composition and mineral modal abundances to Arguin 002, with the northeastern part of the South-Pole Aitken (SPA) basin being the most likely (Supplementary Fig. 9). This launch region satisfies both dynamic[37] and age constraints[22], suggesting that the excavation of noritic lithology from the deep lunar crust (~ 12–20 km) likely occurred contemporaneously with the formation of the SPA basin (Supplementary Text 2.2). Even if the ~ 4.34 Ga age recorded by apatite and zircon reflects a complete resetting of the U-Pb systematics during a large impact event, this age remains consistent with the estimated formation time of the SPA basin within error[22], again supporting an SPA-basin origin for Arguin 002 (Supplementary Text 2.2). Thus, the synchronization of ages and the widespread distribution of Mg-suite rocks, including Arguin 002 and Apollo samples, indicate that a global event likely triggered Mg-suite magmatism between 4.33 and 4.36 Ga.

Lunar dynamics models suggest that gravitational instability-induced mantle overturn of LMO cumulates may have triggered widespread partial melting of the KREEP-free lunar lower mantle, which matches both the estimated abundances of Mg-suite rocks and their global distribution as detected in remote sensing data[6,46,47]. Seismological evidence further supports this global mantle overturn occurring after the crystallization of the LMO[48]. In this context, Mg-suite magmatism could have been rapidly initiated due to gravitational restructuring of the LMO cumulates, potentially driven by the formation of dense, low-viscosity ilmenite-bearing cumulates or even a silicate-driven mantle overturn prior to complete LMO solidification[6,49,50]. This scenario may explain the age overlap between Apollo Mg-suite rocks and Arguin 002, with the age upper bound of lunar mantle overturn potentially constrained by the formation of the primordial lunar crust (~ 4.36–4.37 Ga,[25,51]). Notably, this age coincides with the formation of the oldest Mg-suite rock (Apollo-17 sample 72215) at ~ 4.36 Ga[25], suggesting a short timeframe for the onset of global Mg-suite magmatism in response to mantle overturn. The age disparity between the oldest Mg-suite rock and Arguin 002 further implies that Mg-suite magmatism was a prolonged event, lasting at least 20–30 Myr.

The Chang'e-6 mission, conducted by the China National Space Administration, has successfully sampled lunar surface materials within the SPA basin (41.623°S, 153.917°W). Recent Sr-Nd-Pb isotope analysis of the Chang'e-6 low-Ti basalts reveal compelling evidence for their derivation from a KREEP-free mantle source[52]. Noritic materials have also been identified in the Chang'e-6 regolith breccias[53], consistent with the widespread noritic lithologies observed near the landing site and across the SPA basin[54–56]. Given the possible origin of Arguin 002 near the Chang'e-6 landing site (Supplementary Text 2.2), it is plausible that Arguin 002 shares a genetic correlation with the noritic materials in the region. The increasing number of lunar samples sourced from KREEP-free mantle regions, as exemplified by the Chang'e-6 samples and meteorites[15,20,52], presents an opportunity for deeper insights into Mg-suite magmatism. Future analyses of these samples and their potential genetic links to Arguin 002 could provide critical insights into the timing and spatial distribution of Mg-suite magmatic events, the evolution of the lunar highland crust, and the formation processes of the SPA basin.

Conclusion

Arguin 002 is the first unbrecciated, chemically pristine, fresh whole-rock meteorite definitively identified as an Mg-suite norite. Detailed petrological, mineralogical, geochemical, and chronological analyses in this study yield the following conclusions:

(1) The mineral assemblages of Arguin 002 likely formed through high-degree (> 90 %) fractional crystallization of a primary magma generated by low-degree (< 2 %) partial melting of the KREEP-free lower lunar mantle. This finding suggests that lunar Mg-suite magmatism is not necessarily driven by or associated with KREEP components.

(2) The KREEP-free Mg-suite rocks, exemplified by Arguin 002, likely have an endogenous plutonic origin. Their parental magma may have intruded into the lunar crust at depths of ~ 12–20 km before being excavated by a large basin-forming impact, such as that created the SPA basin.

(3) The crystallization age of Arguin 002 (4341.5 ± 9.3 Ma), aligns with the ages of Apollo Mg-suite and related rocks, supporting the hypothesis that Mg-suite magmatism was a global, nearly synchronous event driven by mantle overturn. The lunar Mg-suite magmatism persisted for at least 20–30 Myr.

Methods

Structural and chemical characterizations of minerals

The mineral modal abundances of Arguin 002 were analyzed using the TESCAN Integrated Mineral Analyzer (TIMA) system. The microstructure of the sample was examined using an electron microprobe equipped with a Cathodoluminescence (CL) imaging detector. Raman spectrometry was employed to identify the spectral characteristics of the minerals within the sample. Additionally, the major and trace element compositions of the mineral phases were determined using an Electron Microprobe Analyzer (EPMA) and Laser Ablation Inductively Coupled Plasma Mass

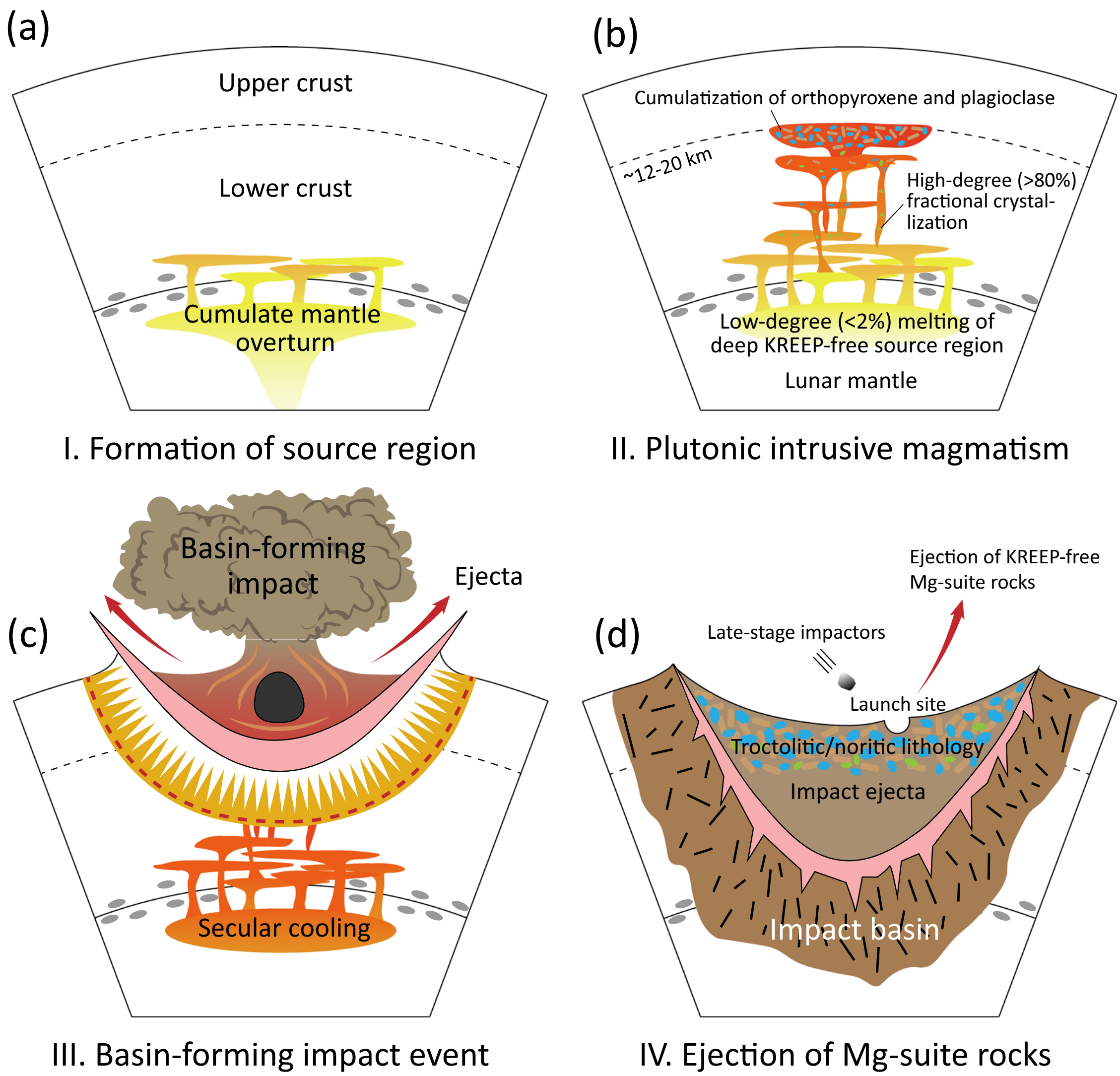

Fig. 6 | A schematic diagram illustrating the endogenous genesis of the lunar meteorite Arguin 002 and related KREEP-free Mg-suite rocks. a A KREEP-free primary melt forms via partial melting of the deep lunar mantle, potentially triggered by mantle overturn. **b** The partial melt undergoes fractional crystallization and intrudes into the lunar crust, where it slowly cools to form noritic cumulates. **c** A major impact event transports these noritic materials to the lunar surface, producing ejecta. **d** A subsequent impact event propels KREEP-free Mg-suite rocks from the lunar surface to Earth.

Spectrometry (LA-ICP-MS), respectively. For detailed descriptions and accuracies of these methods, readers are referred to Supplementary Text 1.

Mineral trace-element analysis

Trace-element concentrations of minerals in the sample were analyzed using LA-ICP-MS at the Wuhan SampleSolution Analytical Technology Co., Ltd., Wuhan, China. Details of the operating conditions for laser ablation and ICP-MS instruments, as well as data reduction procedures can be found in[57]. A GeolasPro laser ablation system, comprised of a COMPexPro 102 ArF excimer laser (193 nm wavelength; 200 mJ max energy) and a MicroLas optical setup, was employed for laser sampling. Atoms were ionized and ion-signal intensities were registered using an Agilent 7900 ICP-MS instrument equipped with a secondary electron multiplier. Helium served as the carrier gas, and argon, utilized as the supplementary gas, was introduced via a T-connector prior to ICP entry. The laser operational settings were adjusted to 44 µm spot size, 80 mJ energy, and 5 Hz frequency. A range of reference materials (BCR-2G, BHVO-2G, BIR-1G, and GSE-1G) were employed to calibrate trace element concentrations[58]. Analysis of each spot included a background acquisition of approximately 20–30 s followed by 50 s of data acquisition of the sample. ICPMSDataCal, an Excel-based software, was used off-line for selection and integration of background and analyzed signals, time-drift correction, and quantitative calibration[58]. Results for the reference materials, detailed in Supplementary Data 2, are consistent with the GeoReM database, showing relative errors of $< 10\%$ (mostly $< 5\%$) for key elements (e.g., Sc, Th, and REEs) analyzed in this study.

Bulk-rock major- and trace-element analysis

To ensure representative sampling, three chips from different parts of the whole rock, each weighing ~1 g, were crushed to particles smaller than 70 µm using an agate mortar. Then, 40 mg of powder was randomly sampled from each of the three ~1 g portions of powder for analysis. To ensure consistent test results between testing agencies, one powder sample was analyzed at Nanjing FocuMS Technology Co. Ltd, and the other two at China University of Geosciences Beijing. In each testing agency, the crushed sample was digested in a high-pressure PTFE bomb with 0.5 ml of 60 wt% HNO_3 and 1.0 ml of 40 wt% HF. The bomb was then placed in an oven at 195 °C for 3 days to ensure complete digestion. After cooling and drying, the sample was mixed with 1 ml of Rh internal standard solution and re-dissolved in 5 ml of 15 wt% HNO_3 in the oven at 150 °C overnight. Aliquots of the dissolved sample were prepared for analysis: one (2000 × dilution) for trace elements, analyzed using an Agilent Technologies 7700x quadrupole

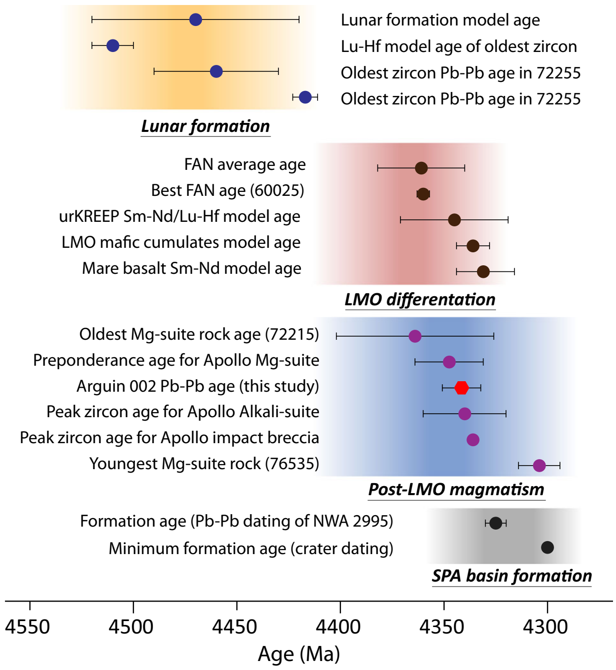

Fig. 7 | Schematic diagram summarizing important age anchors for lunar formation, LMO differentiation, post-LMO magmatism, and formation of South-Pole Aitken (SPA) basin. The chronological data from[22,25,26,73,74] (and references therein) are shown for comparison.

ICP-MS (Tokyo, Japan); and another (500 × dilution) for major elements (excluding silicon), analyzed using an Agilent Technologies 5110 ICP-OES (Penang, Malaysia). The bulk-rock SiO_2 content was calculated by subtracting the combined weights of major and trace element oxides from 100 wt%. USGS geochemical reference materials (BHVO-2 and AGV-2 at Nanjing FocuMS, and AGV-2, GSR-1, GSR-3, and BHVO-2 at China University of Geosciences Beijing) served as quality control benchmarks. The reference material analysis results, detailed in Supplementary Data 2, agree with published data in the GeoReM database, with relative errors of < 10%.

SIMS U-Pb dating

U-Pb isotopic compositions of zircon and phosphates (apatite and merrillite) in Arguin 002 were analyzed using a CAMECA IMS-1280HR ion microprobe at the Institute of Geology and Geophysics, Chinese Academy of Sciences (IGGCAS). Prior to analysis, the sample mounts were coated with a 20-nm-thick gold layer. A Gaussian illumination mode was used to focus a primary beam of $^{16}O^-$ to a diameter of 4 μm. A description of the instruments used for analyses and the analytical procedure can be found in[59] and[60] for zircon and in[61] for phosphates, and only a brief summary is provided here.

The first session focused on the U-Pb isotope measurement of zircon. A single electron multiplier was used in ion-counting mode to measure secondary-ion beam intensities by a peak jumping sequence, with each measurement consisting of seven cycles. Measured U-Pb ratios were corrected for U oxides using the power-law relationship between $^{206}Pb/^{238}U$ versus $^{238}U^{16}O_2/^{238}U$ of reference zircon Plešovice. A second standard, GBW04705 (Qinghu), was also analyzed with zircon grains as an unknown. Long-term uncertainty for the $^{206}Pb/^{238}U$ measurements of the standard zircons was propagated to the unknowns (1 relative standard deviation (RSD) = 1.5%).

The second session focused on the U-Pb isotope measurement of phosphates. A multi-collector mode with five electron multipliers was used. A hybrid dynamic multicollector technique with five detectors was used to determine the ion beam intensities of $^{204}Pb^+$, $^{206}Pb^+$, $^{207}Pb^+$, $^{238}U^+$, $^{232}Th^{16}O^+$, $^{238}U^{16}O^+$, and a matrix reference peak of $^{40}Ca_2{}^{31}P^{16}O_3{}^+$ at a mass resolution of 7000 (defined at 50% height). The $^{206}Pb^+$ peak was used as a reference peak for centering the secondary ion beam, energy, and mass calibration. NIST610 glass was used to calibrate the relative yield of different electron multipliers and evaluate the external reproducibility of Pb isotopic compositions. Pb/U ratios were calibrated with a power law relationship between $^{206}Pb/^{238}U$ and $^{238}U^{16}O/^{238}U$ relative to an apatite standard of NW-1.

After measurement, data reduction was carried out using the Isoplot 3.0 program[28]. An average present-day crustal Pb isotopic composition was used for terrestrial common Pb correction[62].

Mantle melting and fractional crystallization modeling

It has been demonstrated that the major elemental compositions of primary melts for KREEP-poor/free Mg-suite troctolites can be produced by low-degree (~ 1–2%) batch melting at ~ 2.1 GPa within the cumulate lunar mantle, formed through ~ 50% equilibrium crystallization of an LMO with a "lunar primitive upper mantle" (LPUM) initial composition[21]. This study investigates whether the REE patterns and contents of Arguin 002 and KREEP-free Mg-suite-related clasts in lunar meteorites could also arise from this process.

To test this hypothesis, we applied a geochemical model to calculate the REE concentrations in the mantle source, the primary melts, and the parental magmas of KREEP-free Mg-suite rocks, accounting for both partial melting and fractional crystallization processes. The model comprises four steps, as described below in detail.

(1) Modeling of mantle source composition: We modeled the bulk REE composition of the mantle source for KREEP-free Mg-suite rocks, formed from the solidification of an LPUM LMO with an initial REE composition of ~ 2.7 × CI chondrites[63]. Following the crystallization protocol in[1], we used equilibrium crystallization equations to calculate the REE contents of LMO cumulates and residual liquid:

$$C_L = \frac{C_{LMO}}{F + D(1 - F)}, C_S = DC_L \tag{1}$$

where D is the total partition coefficient of REE between mantle cumulates and residual liquid, F is the crystallization degree, and C_{LMO}, C_L, and C_S are the REE contents of the initial LMO, residual liquid, and fractionated solids, respectively. REE partition coefficients were sourced from[63]. After 50% equilibrium crystallization of the LMO, with ~ 3% trapped instantaneous residual liquid (TIRL)[1], the resulting mantle source comprised primarily olivine, with La and Lu contents of 0.17 × and 0.34 × CI chondrites, respectively.

(2) Modeling of primary melt composition: We calculated the REE concentrations of a low-degree (~ 1–2%) partial melt from this mantle source by batch melting, assuming each mineral phase melts in proportion to its modal abundance, as outlined in[64,65]. The batch melting equation is similar to Eqn. (1), with the only differences being that C_{LMO} is replaced by C_L, and F represents the batch melting degree. The batch melting produced a primary melt with relatively flat REE contents from La (16.0 × CI chondrites) to Lu (7.8 × CI chondrites) (1% partial melting), or from La (8.2 × CI chondrites) to Lu (6.4 × CI chondrites) (2% partial melting).

(3) Modeling of parental magma compositions: Since Mg-suite rocks are mostly cumulate rocks and their bulk compositions do not reflect parental magma compositions, we reconstructed the REE contents of their parental magmas using REE concentrations in silicate minerals (plagioclase, clinopyroxene, and orthopyroxene) and partition coefficients between these minerals and melts. For consistency, REE partition coefficients were again sourced from[63]. Besides Arguin 002, we determined the parental magmas of KREEP-free Mg-suite-related clasts from NWA 7611[27], NWA 10401[15], NWA 10986[18], and NWA 11788[20] using the same approach.

(4) Modeling of fractional crystallization of primary magma: To predict the REE contents of KREEP-free Mg-suite parental magmas, we

modeled the fractional crystallization of the primary magma using the following equation:

$$C_{LR} = C_L(1 - F)^{D-1} \quad (2)$$

where C_{LR} is the REE content of the residual melt after fractional crystallization, and F is the degree of mineral fractionation. The mineral fractionation scheme follows the results in[21] and is summarized here. Before the fractionation degree reaching 87 wt%, the magma first fractionates olivine then co-crystallizes olivine and plagioclase, forming troctolitic lithology. At fractionation degree > 87 wt%, orthopyroxene begins to crystallize and thus forms noritic lithology. For Arguin 002, the formation of noritic lithology with an observed pyroxene Mg# range of 65.5–69.0 corresponds to a fractionation degree of > 95 wt%[21]. If the fractional crystallization modeling in such a range of fractionation degree can reproduce the REE contents and patterns of the parental magma of Arguin 002 calculated in the step (3) within error range, we can infer that the lithology of Arguin 002 likely formed through the aforementioned processes, suggesting a possible genetic relationship with KREEP-free Mg-suite troctolites, as expected by[21].

The MATLAB codes for implementing the four-step modeling process are provided in this study. For detailed instructions on the implementation process, please refer to the *Code Availability Statement* section.

Launch site identification

The procedure for identifying the possible launch sites of Arguin 002 included two steps. First, the bulk-rock chemical composition measured for Arguin 002 was compared with a global dataset of lunar surface chemical compositions. This dataset consist of high-resolution (~ 59 m/pixel) maps of key elemental oxides (i.e., Al_2O_3, CaO, FeO, MgO, and TiO_2) spanning a latitude range between ± 65°[66] and a global Th map[67]. Possible launch sites were preliminarily selected based on matching between the spectral and meteorite elemental contents considering their uncertainties. For the meteorite elemental data, the highest and lowest values measured in the three parallel bulk-rock ICP-MS measurements were used as the error range. For the remote sensing data, estimated errors of ± 2 wt% for MgO and CaO, ± 1 wt% for Al_2O_3 and FeO, ± 0.5 wt% for TiO_2, 2 ppm for Th were applied to reflect the prediction accuracy of individual oxide content on the lunar surface. Based on these selections, in the second step, a global dataset of lunar surface mineral abundances was used to further select source sites that match the modal mineral abundances observed in the meteorite. The global mineral abundance datasets were created from reflectance data obtained by the Mineral Mapper of the JAXA SELENE/Kaguya mission and corrected for topography, with a spatial resolution of ~ 59 m/pixel and covering latitudes between ± 50°[68]. To ensure comparability with the remote sensing datasets, modal abundances of major phases, including clinopyroxene, orthopyroxene, plagioclase, and impact melt in the meteorite sample were first normalized to a sum of 100%. Because the impact melt (modal abundance 10.1%) in the meteorite has a chemical composition representing a mixture of pyroxene and plagioclase with unknown proportions, they add significant uncertainties to the mineral abundances in the pre-shock rock. For this reason, a ± 10.1% total uncertainty was assigned to the modal abundances of pyroxene and plagioclase when making the comparison, resulting in the following matching thresholds: 38.3–58.4% for orthopyroxene, 0–14.8% for clinopyroxene, and 26.8–47.0% for plagioclase. Given the absence of olivine in the meteorite sample, only the sites with an olivine content < 8% were considered as potential source sites for Arguin 002, based on the fitting error of the global mineral abundance dataset[69]. The implementation of these two steps was carried out using the "Map Algebra" toolbox in ArcGIS 10.8 software.

Data availability

The instrument analysis data used this study are available in the Supplementary Files and the Zenodo repository[70].

Code availability

The MATLAB codes used to generate the figures and implement the trace-element partitioning modeling in the main text can be found at: https://github.com/oldkingzlwang/Arguin002_Source_Code.

Received: 17 September 2024; Accepted: 31 January 2025;
Published online: 01 March 2025

References

1. Elardo, S. M., Draper, D. S. & Shearer, C. K. Lunar Magma Ocean crystallization revisited: Bulk composition, early cumulate mineralogy, and the source regions of the highlands Mg-suite. *Geochimica et. Cosmochimica Acta* **75**, 3024–3045 (2011).
2. Elkins-Tanton, L. T., Burgess, S. & Yin, Q.-Z. The lunar magma ocean: Reconciling the solidification process with lunar petrology and geochronology. *Earth Planet. Sci. Lett.* **304**, 326–336 (2011).
3. Shearer, C. K. Thermal and magmatic evolution of the moon. *Rev. Mineral. Geochem.* **60**, 365–518 (2006).
4. Wieczorek, M. A. The constitution and structure of the lunar interior. *Rev. Mineral. Geochem.* **60**, 221–364 (2006).
5. Shearer, C. K. Magmatic Evolution II: a new view of post-differentiation magmatism. *Rev. Mineral. Geochem.* **89**, 147–206 (2023).
6. Prissel, T. C., Zhang, N., Jackson, C. R. M. & Li, H. Rapid transition from primary to secondary crust building on the Moon explained by mantle overturn. *Nat. Commun.* **14**, 5002 (2023).
7. Elardo, S. M. The evolution of the lunar crust. *Rev. Mineral. Geochem.* **89**, 293–338 (2023).
8. Shearer, C. K., Elardo, S. M., Petro, N. E., Borg, L. E. & McCubbin, F. M. Origin of the lunar highlands Mg-suite: An integrated petrology, geochemistry, chronology, and remote sensing perspective. *Am. Mineralogist* **100**, 294–325 (2015).
9. Stadermann, A. C., Barnes, J. J., Erickson, T. M., Prissel, T. C. & Michels, Z. D. Evidence for Extrusive Mg—Suite Magmatism on the Moon? Fine—Grained Magnesian Clasts in an Apollo 16 Impact Melt Breccia. *JGR Planets* **128**, e2022JE007728 (2023).
10. Papike, J. J., Fowler, G. W. & Shearer, C. K. Orthopyroxene as a recorder of lunar crust evolution: An ion microprobe investigations of Mg-suite norites. *Am. Mineralogist* **79**, 796–800 (1994).
11. Papike, J. J., Fowler, G. W., Shearer, C. K. & Layne, G. D. Ion microprobe investigation of plagioclase and orthopyroxene from lunar Mg-suite norites: Implications for calculating parental melt REE concentrations and for assessing postcrystallization REE redistribution. *Geochimica et. Cosmochimica Acta* **60**, 3967–3978 (1996).
12. Shervais, J. W. & McGee, J. J. Petrology of the Western Highland province: ancient crust formation at the Apollo 14 site. *J. Geophys. Res.* **104**, 5891–5920 (1999).
13. Snyder, G. A., Neal, C. R., Taylor, L. A. & Halliday, A. N. Processes involved in the formation of magnesian—suite plutonic rocks from the highlands of the Earth's Moon. *J. Geophys. Res.* **100**, 9365–9388 (1995).
14. Chen, H., Xie, L., Shu, Q. & Miao, B. Northwest Africa 12279: Evidence for the Interaction Between Early Lunar Mantle Melt and Anorthositic Crust. *JGR Planets* **128**, e2023JE007844 (2023).
15. Gross, J. Geochemistry and petrogenesis of Northwest Africa 10401: a new type of the Mg—suite rocks. *JGR Planets* **125**, e2019JE006225 (2020).
16. He, Q. Petrogenesis of magnesian troctolitic granulite clasts from Chang'e -5 drilling sample: Implications for the origin of ejecta material from lunar highlands. *Icarus* **408**, 115853 (2024).
17. Lindstrom, M. M., Marvin, U. B., and Mittlefehldt, D. W. Apollo 15 Mg- and Fe-Norites: A Redefinition of the Mg-Suite Differentiation Trend. In *Proceedings of the 19th Lunar and Planetary Science Conference*, 245–254. Houston (1989).

18. Roberts, S. E., McCanta, M. C., Jean, M. M. & Taylor, L. A. New lunar meteorite NWA 10986: A mingled impact melt breccia from the highlands—A complete cross section of the lunar crust. *Meteorit. Planet. Sci.* **54**, 3018–3035 (2019).
19. Shearer, C. K., Moriarty, D. P., Simon, S. B., Petro, N. & Papike, J. J. Where Is the Lunar Mantle and Deep Crust at Crisium? A Perspective From the Luna 20 Samples. *JGR Planets* **128**, e2022JE007409 (2023).
20. Hulsey, C. R., and O'Sullivan, K. M. Petrographic and geochemical analysis of lunar meteorite NWA 11788: Parallels with Luna 20 and the Apollo magnesian granulites. *Meteori. Planet. Sci.* 59, 2744–2768 (2024).
21. Prissel, T. C. & Gross, J. On the petrogenesis of lunar troctolites: New insights into cumulate mantle overturn & mantle exposures in impact basins. *Earth Planet. Sci. Lett.* **551**, 116531 (2020).
22. Joy, K. H. et al. Evidence of a 4.33 billion year age for the Moon's South Pole-Aitken basin. *Nat. Astron.* 9, 55–65 (2024).
23. Klima, R. L. New insights into lunar petrology: Distribution and composition of prominent low-Ca pyroxene exposures as observed by the Moon Mineralogy Mapper (M3). *J. Geophys. Res.* **116**, E00G06 (2011).
24. Sun, Y., Li, L. & Zhang, Y. Detection of Mg-spinel bearing central peaks using M3 images: Implications for the petrogenesis of Mg-spinel. *Earth Planet. Sci. Lett.* **465**, 48–58 (2017).
25. Borg, L. E., & Carlson, R. W. The Evolving Chronology of Moon Formation. *Annual Rev. Earth Planetary Sci.* **51**, 25–52 (2023).
26. Barboni, M. High-precision U-Pb zircon dating identifies a major magmatic event on the Moon at 4.338 Ga. *Sci. Adv.* **10**, eadn9871 (2024).
27. Cao, H. J. The lithologic diversity of the Moon recorded in lunar meteorites Northwest Africa 7611 and 10480. *Meteorit. Planet. Sci.* **59**, 435–474 (2024).
28. Ludwig, K. *User's manual for Isoplot 3.75*. Berkeley Geochronology Center Special Publication 5, 1–75, (2012).
29. Warren, P. H. The origin of pristine KREEP - Effects of mixing between UrKREEP and the magmas parental to the Mg-rich cumulates. In *Proceedings of the 18th Lunar and Planetary Science Conference* (pp. 233–241). Houston, (1988).
30. Snyder, G. A., Taylor, L. A. & Halliday, A. N. Chronology and petrogenesis of the lunar highlands alkali suite: Cumulates from KREEP basalt crystallization. *Geochimica et. Cosmochimica Acta* **59**, 1185–1203 (1995).
31. Elardo, S. M. & Astudillo Manosalva, D. F. Complexity and ambiguity in the relationships between major lunar crustal lithologies and meteoritic clasts inferred from major and trace element modeling. *Geochimica et. Cosmochimica Acta* **354**, 13–26 (2023).
32. Norman, M. D., Borg, L. E., Nyquist, L. E. & Bogard, D. D. Chronology, geochemistry, and petrology of a ferroan noritic anorthosite clast from Descartes breccia 67215: Clues to the age, origin, structure, and impact history of the lunar crust. *Meteorit. Planet. Sci.* **38**, 645–661 (2003).
33. Takeda, H. Magnesian anorthosites and a deep crustal rock from the farside crust of the moon. *Earth Planet. Sci. Lett.* **247**, 171–184 (2006).
34. Treiman, A. H., and Semprich, J. A Dunite Fragment in Meteorite Northwest Africa (NWA) 11421: A Piece of the Moon's Mantle. *American Mineralog.* 108, 2182–2192 (2023).
35. Sun, L. & Lucey, P. G. Lunar mantle composition and timing of overturn indicated by Mg# and mineralogy distributions across the South Pole-Aitken basin. *Earth Planet. Sci. Lett.* **643**, 118931 (2024).
36. Rapp, J. F. & Draper, D. S. Fractional crystallization of the lunar magma ocean: Updating the dominant paradigm. *Meteorit. Planet. Sci.* **53**, 1432–1455 (2018).
37. Hurwitz, D. M. & Kring, D. A. Differentiation of the South Pole-Aitken basin impact melt sheet: Implications for lunar exploration. *JGR Planets* **119**, 1110–1133 (2014).
38. Vaughan, W. M. & Head, J. W. Impact melt differentiation in the South Pole-Aitken basin: Some observations and speculations. *Planet. Space Sci.* **91**, 101–106 (2014).
39. Prissel, T. C., Parman, S. W. & Head, J. W. Formation of the lunar highlands Mg-suite as told by spinel. *Am. Mineralogist* **101**, 1624–1635 (2016).
40. White, L. F. Evidence of extensive lunar crust formation in impact melt sheets 4,330 Myr ago. *Nat. Astron* **4**, 974–978 (2020).
41. Osinski G R, Grieve R A F, Tornabene L L. Excavation and impact ejecta emplacement. In: *Impact Cratering—Processes and Products*, 43-59, (2020).
42. Grange, M. L., Pidgeon, R. T., Nemchin, A. A., Timms, N. E. & Meyer, C. Interpreting U-Pb data from primary and secondary features in lunar zircon. *Geochimica et. Cosmochimica Acta* **101**, 112–132 (2013).
43. Joseph, C. Towards a new impact geochronometer: Deformation microstructures and U-Pb systematics of shocked xenotime. *Geochimica et. Cosmochimica Acta* **374**, 33–50 (2024).
44. Adcock, C. T. Shock-transformation of whitlockite to merrillite and the implications for meteoritic phosphate. *Nat. Commun.* **8**, 14667 (2017).
45. Zhang, B. D. Timing of lunar Mg-suite magmatism constrained by SIMS U-Pb dating of Apollo norite 78238. *Earth Planet. Sci. Lett.* **569M**, 117046 (2021).
46. Warren, P. H., Wasson, J. T. Early lunar petrogenesis, oceanic and extraoceanic. In *Conference on the Lunar Highlands Crust* (pp. 81–99). Houston, (1980).
47. Hess, P. C. & Parmentier, E. M. A model for the thermal and chemical evolution of the Moon's interior: implications for the onset of mare volcanism. *Earth Planet. Sci. Lett.* **134**, 501–514 (1995).
48. Briaud, A., Ganino, C., Fienga, A., Mémin, A. & Rambaux, N. The lunar solid inner core and the mantle overturn. *Nature* **617**, 743–746 (2023).
49. Maurice, M., Nicola, T., Sabrina, S., Doris, B. & Thorsten, K. A long-lived magma ocean on a young Moon. *Sci. Adv.* **6**, eaba8949 (2020).
50. Chloé, M. & Neufeld, J. A. Formation of the lunar primary crust from a long-lived slushy magma ocean. *Geophys. Res. Lett.* **49**, e2021GL095408 (2022).
51. Sio, C. K., Borg, L. E. & Cassata, W. S. The timing of lunar solidification and mantle overturn recorded in ferroan anorthosite 62237. *Earth Planet. Sci. Lett.* **538**, 116219 (2020).
52. Cui, Z. X. et al. A sample of the Moon's far side retrieved by Chang'e-6 contains 2.83-billion-year-old basalt. *Science*, eadt1093, (2024).
53. Li, C. L. Nature of the lunar far-side samples returned by the Chang'E-6 mission. *Natl Sci. Rev.* **11**, nwae328 (2024).
54. Moriarty, D. P. & Pieters, C. M. The Character of South Pole—Aitken Basin: Patterns of Surface and Subsurface Composition. *JGR Planets* **123**, 729–747 (2018).
55. Pieters, C. M., Head, J. W., Gaddis, L., Jolliff, B. & Duke, M. Rock types of South Pole-Aitken basin and extent of basaltic volcanism. *J. Geophys. Res.* **106**, 28001–28022 (2001).
56. Qian, Y. Long-lasting farside volcanism in the Apollo basin: Chang'e-6 landing site. *Earth Planet. Sci. Lett.* **637**, 118737 (2024).
57. Zong, K. Q. The assembly of Rodinia: The correlation of early Neoproterozoic (ca. 900 Ma) high-grade metamorphism and continental arc formation in the southern Beishan Orogen, southern Central Asian Orogenic Belt (CAOB). *Precambrian Res.* **290**, 32–48 (2017).
58. Liu, Y. S. In situ analysis of major and trace elements of anhydrous minerals by LA-ICP-MS without applying an internal standard. *Chem. Geol.* **257**, 34–43 (2008).
59. Liu, Y., Li, X. H., Li, Q. L., Tang, G. Q. & Yin, Q. Z. Precise U-Pb zircon dating at a scale of <5 micron by the CAMECA 1280 SIMS using a Gaussian illumination probe. *J. Anal. At. Spectrom.* **26**, 845–851 (2011).
60. Ling, X. X. Zircon ZS - a Homogenous Natural Reference Material for U-Pb Age and O-Hf Isotope Microanalyses. *At. Spectrosc.* **43**, 134–144 (2022).

61. Li, Y. & Hsu, W. Multiple impact events on the L-chondritic parent body: Insights from SIMS U-Pb dating of Ca-phosphates in the NWA 7251 L-melt breccia. *Meteorit. Planet. Sci.* **53**, 1081–1095 (2018).
62. Stacey, J. S. & Kramers, J. D. Approximation of terrestrial lead isotope evolution by a two-stage model. *Earth Planet. Sci. Lett.* **26**, 207–221 (1975).
63. Fu, H. R. & Jacobsen, S. B. Earth-Moon refractory element similarity constrains a thoroughly-mixed Moon-forming disk. *Earth Planet. Sci. Lett.* **646**, 119008 (2024).
64. Hallis, L. J., Anand, M. & Strekopytov, S. Trace-element modelling of mare basalt parental melts: Implications for a heterogeneous lunar mantle. *Geochimica et. Cosmochimica Acta* **134**, 289–316 (2014).
65. Srivastava, Y., Basu Sarbadhikari, A., Day, J. M. D., Yamaguchi, A. & Takenouchi, A. A changing thermal regime revealed from shallow to deep basalt source melting in the Moon. *Nat. Commun.* **13**, 7594 (2022).
66. Zhang, L. New maps of major oxides and Mg# of the lunar surface from additional geochemical data of Chang'E-5 samples and KAGUYA multiband imager data. *Icarus* **397**, 115505 (2023).
67. Lawrence, D. J. Thorium abundances on the lunar surface. *J. Geophys. Res.: Planets* **105**, 20307–20331 (2000).
68. Lemelin, M. The compositions of the lunar crust and upper mantle: Spectral analysis of the inner rings of lunar impact basins. *Planet. Space Sci.* **165**, 230–243 (2019).
69. Lemelin, M., Lucey, P. G., Song, E. & Taylor, G. J. Lunar central peak mineralogy and iron content using the Kaguya Multiband Imager: Reassessment of the compositional structure of the lunar crust. *J. Geophys. Res.: Planets* **120**, 869–887 (2015).
70. Wang, Z. L. et al. (2025) Data repository for "Genesis and timing of KREEP-free lunar Mg-suite magmatism indicated by the first norite meteorite Arguin 002". *Zenodo*. https://doi.org/10.5281/zenodo.14710594.
71. Korotev, R. L. & Irving, A. J. Lunar meteorites from northern Africa. *Meteorit. Planet. Sci.* **56**, 206–240 (2021).
72. Korotev, R. L., Zeigler, R. A., Jolliff, B. L., Irvin, A. J. & Bunch, T. E. Compositional and lithological diversity among brecciated lunar meteorites of intermediate iron concentration. *Meteorit. Planet. Sci.* **44**, 1287–1322 (2009).
73. Evans, A. J. Reexamination of early lunar chronology with GRAIL data: terranes, basins, and impact fluxes. *JGR Planets* **123**, 1596–1617 (2018).
74. Zhang, A. C. Isotopic geochronological constraints on the formation and evolution of the moon. *Space Sci. Technol.* **4**, 0170 (2024).

Acknowledgements
We greatly appreciate thorough and constructive reviews from Prof. Joshua Snape and the other anonymous reviewer, and careful editorial works from Prof. Ke Zhu and Dr. Joe Aslin. We are especially grateful to Paul H. Warren for his very detailed, constructive comments and discussions. Our thanks also go to Dr. Ziyao Wang for providing the samples essential for this study and to Dr. Hongxia Ma for her diligent work in sample pretreatment. We acknowledge the support of Prof. Zhenyu Chen and Dr. Haiping Ren for their assistance with the EPMA and TIMA analyses, respectively. Special thanks are extended to Dr. Jiao Li and Dr. Xiaoxiao Ling for their contributions to the SIMS experiments and subsequent data analysis. We are also grateful to Prof. Qiuli Li for engaging in discussions and offering interpretations of the work. This study was supported by the National Natural Science Foundation of China (No. 42272348 & 424B2020).

Author contributions
Z.L.W. and W.T. initiated the research and formulated the core ideas. W.-R.W. and T.C.P. contributed to broadening the scope of this work. Y.K.D. carried out U-Pb age calculations and their interpretations. Y.Q.Q. conducted analyses matching whole-rock compositions with lunar-surface spectral data and provided interpretations based on remote sensing. P.P.L. and W.Z.F. contributed to refining these concepts. Z.L.W., W.-R.W. and A.S. conducted the petrological, mineralogical, and geochemical analyses. Z.L.W. led the analysis and interpretation of the results and drafted the manuscript with contributions from Y.Q.Q. and Y.K.D. W.T., W.-R.W., T.C.P., P.P.L. and W.Z.F. thoroughly reviewed, revised, and proofread the manuscript.

Competing interests
The authors declare no competing interests.

Additional information
Supplementary information The online version contains supplementary material available at https://doi.org/10.1038/s43247-025-02086-7.

Correspondence and requests for materials should be addressed to Wei Tian.

Peer review information *Communications Earth & Environment* thanks Joshua Snape and the other, anonymous, reviewer(s) for their contribution to the peer review of this work. Primary Handling Editors: Ke Zhu and Joe Aslin. A peer review file is available.